Ab initio study on the structural characteristics of amorphous Zn2SnO4

Joohwi Lee, Youngho Kang, Seungwu Han, Cheol Seong Hwang, and Jung-Hae Choi

Citation: Appl. Phys. Lett. **103**, 252102 (2013); doi: 10.1063/1.4850895
View online: http://dx.doi.org/10.1063/1.4850895
View Table of Contents: http://apl.aip.org/resource/1/APPLAB/v103/i25
Published by the AIP Publishing LLC.

Ab initio study on the structural characteristics of amorphous Zn_2SnO_4

Joohwi Lee,[1,2,3] Youngho Kang,[2] Seungwu Han,[2] Cheol Seong Hwang,[2,3] and Jung-Hae Choi[1,a)]

[1]*Electronic Materials Research Center, Korea Institute of Science and Technology, Seoul 136-791, South Korea*
[2]*Department of Materials Science and Engineering, Seoul National University, Seoul 151-744, South Korea*
[3]*Inter-University Semiconductor Research Center, Seoul National University, Seoul 151-744, South Korea*

(Received 25 September 2013; accepted 3 December 2013; published online 16 December 2013)

The structural characteristics of amorphous Zn_2SnO_4 were investigated using *ab initio* calculations in comparison with its crystalline phase. By amorphization, both the coordination number of Zn and the most probable bond length of Zn-O decreased, and the O-Zn-O angle distribution became broader. Meanwhile, the coordination number of Sn was almost unchanged, and the reducing tendency in the most probable bond length of Sn-O as well as the extent of broadening in the O-Sn-O angles were less distinct. The significant changes in Zn-O bonds by amorphization partly account for the higher crystallization temperature of Zn_2SnO_4 compared to its binary oxides. © *2013 AIP Publishing LLC*. [http://dx.doi.org/10.1063/1.4850895]

Zinc tin oxide is a transparent oxide semiconductor (TOS) which shows high optical transparency and controllable electrical conductivity, making it a strong candidate as the semiconductor layer in electronic devices, such as displays, solar cells, and electrical memory devices.[1–4] For the application of TOS in thin film transistors (TFTs), the amorphous phase is preferred for better uniformity over a large area of cell arrays because there are no problems related to grain boundaries. The performance of TFT devices with an amorphous channel was reported to be improved by thermal annealing at a relatively high temperature presumably due to the decrease of localized defect states.[5,6] Therefore, maintaining an amorphous structure at temperatures as high as possible is crucial for the fabrication of high-performance TFT devices. Zinc tin oxide is known to remain as amorphous phase up to 650 °C, which is much higher than the crystallization temperature of its binary oxides of ZnO or SnO_2 (250–300 °C).[6–8] To understand the reason for the high crystallization temperature of the ternary zinc tin oxide compared with its binary constituents, understanding the structural characteristics of crystalline and amorphous phases on the atomic scale is necessary.

One of the leading transparent oxide semiconductors, indium gallium zinc oxide (IGZO) also shows high crystallization temperature of approximately 600 °C (Ref. 9), and several studies examined its amorphous structures and electrical properties by the *ab initio* calculations.[9–13] However, they did not pay attention to the correlation between the structural characteristics and the high crystallization temperature.

In this study, the structural characteristics of both crystalline and amorphous phases of zinc tin oxide were investigated by *ab initio* calculations. The radial distribution function (RDF) and angular distribution function (ADF) were obtained to compare the bond characteristics of the crystalline and amorphous phases.

All the calculations based on density functional theory were performed using the Vienna *Ab initio* Simulation (VASP) Package.[14,15] For the crystalline phases, Zn_2SnO_4 (c-ZTO) of both the tetragonal structure ($P4_122$) and the monoclinic structure (P1) in the inverse spinel type were employed. Note that the occupancy of the octahedral sites by Zn and Sn in the tetragonal structure is ordered while it is random in the monoclinic structure.

Amorphous phase having the atomic ratio of Zn: Sn: O = 2:1:4 (a-ZTO) was obtained with supercells composed of 56, 112, and 224 atoms. The amorphous structures were obtained by a two-step process; melt-quenching by *ab initio* molecular dynamics (AI-MD) simulations and subsequent structure optimization by static calculations. For efficiency during the AI-MD simulation, looser conditions were applied with the cutoff energy of 300 eV, soft pseudo-potential for oxygen, and Γ-only *k*-point sampling. The projector augmented wave (PAW) method,[16] within the generalized gradient approximation (GGA) parameterized by Perdew *et al.* (PBE),[17] was used. Considering the density reduction during amorphization, the volume of the a-ZTO was kept at 106% of the volume of the c-ZTO ($P4_122$) with the cubic shape under the number-volume-temperature (NVT) ensemble.[18] Randomization of the structure was performed at 5000 K for 2 ps with a time step of 2 fs. Then, melting was performed at 2500 K for 10 ps, which is the typical method to obtain amorphous structures. Note that 2500 K is higher than the melting temperatures of individual binary oxides.[19,20] Finally, the structure was quenched from 2500 to 300 K at cooling rates of 25, 50, and 100 K/ps.

For the optimization of the amorphous structure, tight conditions were applied with the cutoff energy of 500 eV, hard pseudo-potential for oxygen as in the crystalline structures. $2 \times 2 \times 2$ Γ-centered *k*-space sampling was chosen for all amorphous supercells. The full relaxation of the atomic positions was performed until the Hellmann–Feynman force on each atom was reduced below 0.03 eV/Å and the external pressure fell below 0.05 GPa. On-site Coulombic interactions (GGA+U) were additionally applied in the

a)Author to whom correspondence should be addressed. Electronic mail: choijh@kist.re.kr. Tel.: +82 2 958 5488. Fax: +82 2 958 6658.

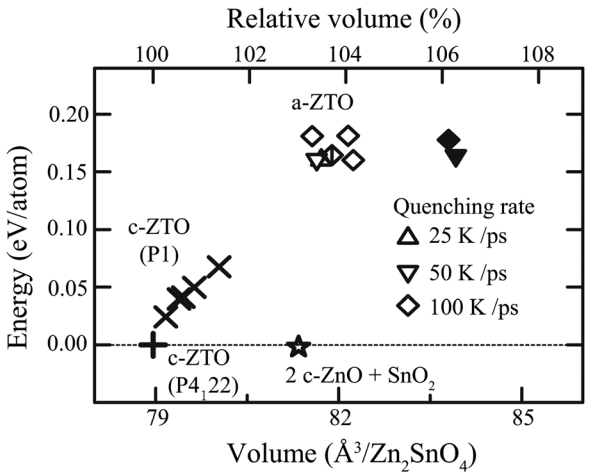

FIG. 1. Energy-volume diagram for various ZTOs. The reference structure of the energy and volume is c-ZTO (P4$_1$22). Closed, open, and open mark with the vertical line correspond to the amorphous cells composed of 56, 112, and 224 atoms.

structure optimization step to address the underbinding of the *d* orbitals of Zn or Sn within the conventional GGA methods.[21,22] The effective U values of 7.5 eV for Zn and 3.5 eV for Sn were used by referring to previous reports on the binary oxides.[23,24] As references, binary oxides of ZnO and SnO_2 were also investigated. For crystalline phases, ZnO in the wurtzite structure and SnO_2 in the rutile structure were used, and their amorphous phases were obtained with supercells composed of 72 atoms.

The structural characteristics were analyzed using RDFs and ADFs. Coordination numbers (CNs) and bond lengths were counted from the RDF using the cutoff radius of 2.55 Å which is the first minimum after the first peak in the RDF for a-ZTO. To understand the distribution of the bond lengths in the amorphous phase, both the mean bond length and the mode bond length were considered. The mean value is defined as $\frac{1}{n}\sum_{i=1}^{n} x_i$, where x_i is the bond length and n is the total number of bonds, while the mode value is defined as the bond length where the maximum peak of RDF is obtained, i.e., the most frequent bond length.

Fig. 1 shows the energy-volume diagram for c-ZTOs and a-ZTOs. The energy of the separated phases of (2c-ZnO + c-SnO_2) was also included for comparison and showed the lowest energy value (star symbol). The c-ZTOs belonging to different space groups in the unit-cell scale (P4$_1$22 and five P1 structures) and eight amorphous phases obtained with various quenching rates and numbers of atoms in the supercells were investigated. Due to the different octahedral occupancy by Zn and Sn, various c-ZTO structures show substantial variations in the volume and energy. The most stable c-ZTO structure was P4$_1$22, as in previous reports;[25,26] therefore, it was selected as a reference in this work. The P4$_1$22 structure was composed of 8 Zn, 4 Sn, and 16 O atoms, and its lattice parameters a (=c) and b were calculated to be 6.077 and 8.551 Å, respectively.

The energies of the a-ZTOs were 0.15–0.17 eV/atom higher than that of the reference c-ZTO and higher than those of metastable c-ZTOs (P1), irrespective of the quenching rate and the number of atoms in the supercell. The volume of the a-ZTOs, however, depends on the size of the supercell. The volumes of supercells composed of 56 atoms were 2%–3% larger than those composed of 112 and 224 atoms. Although the CN and the bond length were found to be qualitatively insensitive to supercell size, the 56 atom-supercells were not included for further analyses for this reason. The volumes of the supercells composed of 112 and 224 atoms were 3%–4% larger than that of the reference c-ZTO. The increases in energy and volume of a-ZTOs compared to the c-ZTO are comparable to the previous calculation results on other multi-component amorphous oxide semiconductor systems, such as InZnO, $InGaZnO_4$, and $InAlZnO_4$.[10]

Figs. 2(a) and 2(b) show the RDFs of Zn-O and Sn-O for a-ZTOs, respectively, which were obtained by averaging over six amorphous supercells. The vertical solid and dashed lines in the inset figure indicate mean bond lengths between O and metal atoms at the tetrahedral and octahedral sites in the P4$_1$22 structure, respectively. The black and gray lines in the inset figure indicate the mean bond lengths between O and metal atoms in c-ZTO and crystalline binary oxides, respectively. The details of the bond length and the coordination number for ZTOs are summarized in Table I in comparison with those in ZnO and SnO_2. The RDFs for the a-ZTO clearly show that only the short range order exists, as indicated by the strong first peak and broad dispersion at longer distance, which is similar to $InGaZnO_4$, $InAlZnO_4$, and In_2ZnO_4.[10]

In Fig. 2(a), the mean bond length of Zn-O of the tetrahedral site in c-ZTO is similar to that in c-ZnO (0.03 Å

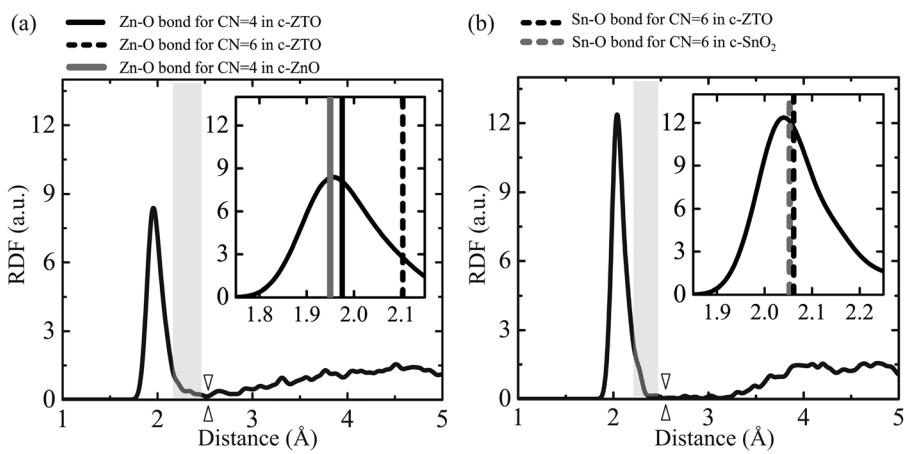

FIG. 2. RDFs of (a) Zn-O and (b) Sn-O in a-ZTO. Inset represents the enlarged first peak in the RDF for easy viewing. The vertical solid and dashed lines in the insets indicate the mean bond lengths between O and metal atoms at the tetrahedral and octahedral sites, respectively. The vertical black and gray lines in the insets represent the mean bond lengths between O and metal atoms in c-ZTO and c-ZnO or c-SnO_2, respectively. The shaded region denotes the tails of longer bonds and the up-and-down triangle denotes the cutoff radius.

TABLE I. CN and bond length in Å for crystalline and amorphous ZTO, ZnO, and SnO_2.

	c-ZTO		a-ZTO		c-ZnO or c-SnO_2		a-ZnO or a-SnO_2	
	CN	Bond length[a]	CN	Bond length[a]	CN	Bond length[a]	CN	Bond length[a]
Zn(-O)	4	1.98 ± 0.03 (2×1.95, 2×2.00)	4.43 ± 0.06	2.01 ± 0.12 (1.96)[b]	4	1.95 ± 0.01	3.89 ± 0.14	1.96 ± 0.08 (1.94)[b]
	6	2.10 ± 0.09 (2×2.02, 2×2.09, 2×2.19)						
Sn(-O)	6	2.06 ± 0.04 (2×2.02, 2×2.07, 2×2.10)	5.89 ± 0.11	2.09 ± 0.09 (2.04)[b]	6	2.05	6.04 ± 0.02	2.09 ± 0.09 (2.05)[b]
O(-Zn)	2	…	2.21 ± 0.03	…	4	…	3.89 ± 0.14	
O(-Sn)	2	…	1.47 ± 0.03	…	3	…	3.02 ± 0.02	

[a]Mean values with the standard deviations are represented.
[b]Mode values for amorphous are in parentheses.

difference); however, it is about 0.1 Å shorter than that of the octahedral site, which shows that the higher the coordination number, the longer the bond length is. For a-ZTO, the first peak in the RDF, which corresponds to the mode bond length of Zn-O, is almost identical to the mean bond length of Zn-O in c-ZnO and slightly shorter than that in c-ZTO. The RDF demonstrates that the Zn-O bonds in a-ZTO prefer the tetrahedral site-like configuration, following the bond character in binary oxide of ZnO. In fact, the mean CN of Zn in a-ZTO was estimated to be 4.43, which decreased from 5 in c-ZTO and approached 4 in c-ZnO.

Fig. 2(b) shows the RDF for the Sn-O bonds in a-ZTO compared to the mean bond lengths of Sn-O in c-ZTO and c-SnO_2 (inset figure). Unlike Zn atoms, all Sn atoms in both c-ZTO and c-SnO_2 are located at the octahedral sixfold-coordinated sites, and the mean bond length of Sn-O is almost identical to those in both c-ZTO and c-SnO_2. Note that the mode bond length of Sn-O for a-ZTO is slightly shorter than the mean bond lengths in c-ZTO and c-SnO_2. The mean CN of Sn in a-ZTO was 5.89, which shows a much smaller decrease from those in c-ZTO and c-SnO_2 compared to the case of Zn. A slight contraction of the metal-oxygen bond length was also found in amorphous In_2ZnO_4.[10]

When the shape of the first peak in the RDF of amorphous phase is completely symmetric, the mode value and the mean value of the bond length are exactly identical. However, the mean bond lengths of Zn-O and Sn-O were about 0.05 Å and 0.02 Å longer than the mode values due to the long tails after the first peak (shaded region in Fig. 2). This indicates that some bonds were elongated and weakened by amorphization. These long bonds induce the volume increase in a-ZTO compared to c-ZTO. On the other hand, the preference for tetrahedral-like sites by Zn atoms accounts for the shortening of the most frequent bond length in a-ZTO.

The CNs and the bond lengths of the amorphous binary oxides were also compared as references. The cutoff distances extracted from the first minima of the RDF were shorter than that in a-ZTO, and they were 2.35 Å for Zn-O in a-ZnO and 2.42 Å for Sn-O in a-SnO_2, respectively. The CNs of Zn for a-ZnO and Sn for a-SnO_2 were almost identical to their crystalline correspondence; four for c-ZnO and six for c-SnO_2, respectively. The mean bond lengths in the amorphous binary oxides were slightly longer than their crystalline correspondences. On the other hand, the mode bond lengths in a-ZnO and a-SnO_2 were almost identical to the mean bond lengths in c-ZnO and c-SnO_2, which is a different tendency from that of a-ZTO.

Figs. 3(a) and 3(b) show the ADFs of O-Zn-O and O-Sn-O for a-ZTO, respectively. The bond angles of 109.5° and 90°, which correspond to the ideal tetrahedral and octahedral sites, are represented by vertical dashed lines. The angles formed by the three atoms in the crystalline phase were fixed and are represented as the vertical solid lines. Note that the bond angles in the crystalline phases slightly deviate from the ideal values due to atomic relaxation. On the other hand, the bond angles in a-ZTO are highly dispersed from those in c-ZTO. The O-Zn-O angles show much broader distributions than the O-Sn-O angles. This can be ascribed to the dual

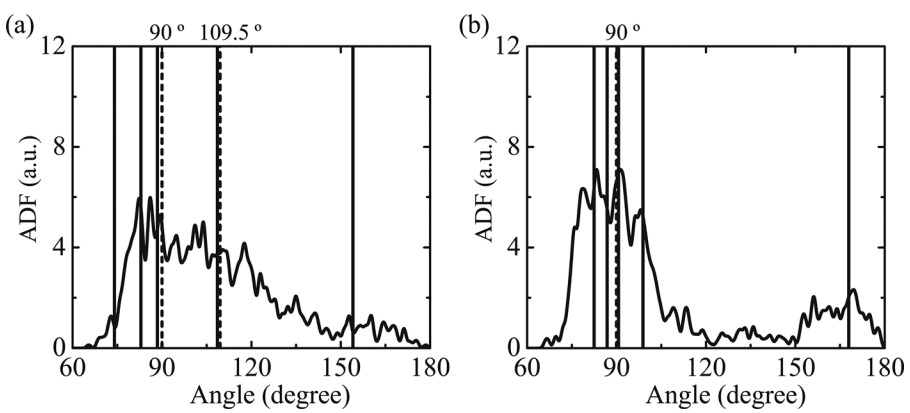

FIG. 3. ADFs of (a) O-Zn-O and (b) O-Sn-O in a-ZTO. Vertical solid and dashed lines indicate the angles of c-ZTO, and the bond angles of the ideal tetrahedral and octahedral sites, respectively.

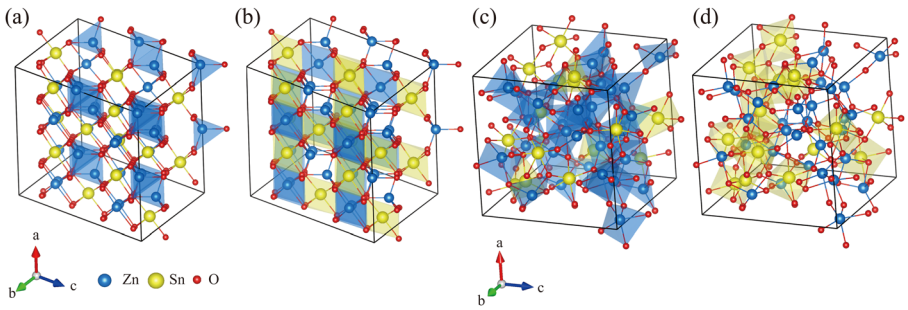

FIG. 4. Atomic structures showing (a) oxygen tetrahedra in c-ZTO, (b) oxygen octahedra in c-ZTO, (c) oxygen tetrahedra or bi-pyramids in a-ZTO, and (d) oxygen octahedra in a-ZTO. Blue and yellow polyhedra indicate those surrounding Zn and Sn atoms, respectively.

preference of Zn for tetrahedral and octahedral sites c-ZTO. In addition, some Zn atoms were observed to bond with five O atoms, forming a bi-pyramid (ZnO_5) which has the bond angle of 120°; therefore, the angle distribution became wider and more irregular. This bi-pyramidal Zn-O was experimentally found in other TOSs, such as crystalline and amorphous InGaZnO.[27,28] Some amorphous phases having predominantly ionic bond character, such as TiO_2, showed wide dispersion in the ADF like a-ZTO (Ref. 29) whereas several other amorphous phases with predominantly covalent bond character, such as SiO_2 showed narrower dispersion in ADF than a-ZTO.[30]

Fig. 4 shows the atomic structures of the c-ZTO and a-ZTO composed of 112 atoms with the oxygen polyhedra with the metal atoms in the center. The atomic configurations and the oxygen polyhedra were illustrated by Visualization for Electronic and Structural Analysis (VESTA).[31] Figs. 4(a) and 4(b) show the oxygen tetrahedra and octahedra in c-ZTO, respectively. The c-ZTO is a $2 \times 1 \times 2$ supercell of the primitive tetragonal ($P4_122$) ZTO cell. In c-ZTO, half of the Zn atoms are surrounded by oxygen tetrahedra while the other half of the Zn atoms are surrounded by oxygen octahedra, which follows the crystal structure of the inverse spinel. All Sn atoms are surrounded by oxygen octahedra. On the other hand, Fig. 4(c) shows the oxygen tetrahedra and bi-pyramids while Fig. 4(d) shows the oxygen octahedra in a-ZTO. Note that all Zn atoms are surrounded by oxygen tetrahedra or bi-pyramids while all oxygen octahedra are found around Sn atoms in a-ZTO. The obvious decrease in the number of oxygen octahedra surrounding Zn atoms were observed for all the amorphous supercells, regardless of the quenching rate and supercell size, although some amorphous supercells contain one or two oxygen octahedra surrounding Zn atoms. Furthermore, the oxygen polyhedra in a-ZTO deviate from the regular polyhedra, indicating the broad distribution of the atomic angles. These atomic structures clearly show a decrease in the CN of Zn and broad angle distributions in a-ZTO.

Generally, higher crystallization temperature is expected for a ternary oxide than its constituent binary oxides due to the longer and complex diffusion path. However, indium tin oxide was reported to show low crystallization temperature of 160–170 °C.[32] Therefore, the computational results in this study suggest that the higher crystallization temperature of ZTO compared to its binary oxides can be attributed to several features on the atomic structure around Zn. First, for crystallization, the CN of about half of the Zn atoms should increase to six, which is accompanied by an increase in the bond length. Second, if the phase separation occurs into the mixture of ZnO and SnO_2,[6,26] it needs additional diffusion of Zn and Sn atoms by breaking and forming bonds with O atoms. For these reasons, the activation barriers for ZTO to crystallize are thought to be higher than those of its binary oxides. Diversity in the CN of Zn and the bond length of Zn-O have also been reported for various crystalline phases of zinc tin oxide including Zn_2SnO_4 and $ZnSnO_3$.[26,33] High crystallization temperatures were also observed for other TOSs having Zn as one of the constituent atoms, such as InZnO, InGaZnO, and InZnSnO,[9,34,35] and the dual occupancy of Zn at tetrahedral and bi-pyramidal sites were reported.[9,35] In these materials, the reduction in the CN of Zn toward four in amorphous phase was observed experimentally by the extended X-ray absorption fine structure.[27,33]

In summary, the structural characteristics of crystalline and amorphous Zn_2SnO_4 (c-ZTO and a-ZTO) were investigated by *ab-initio* calculation. In a-ZTO, the mode bond length of Zn-O became slightly shorter than the mean bond lengths of Zn-O in c-ZTO and c-ZnO, and the mean CN of Zn was also reduced and approached that of c-ZnO. Considering the similarity of the bond lengths of Sn-O and CN of Sn among various phases, the high crystallization temperature of ZTO is mainly attributed to the large variation of Zn-O bond structures between c-ZTO and a-ZTO. Such a relatively high energy barrier for the crystallization of a-ZTO confirms the structural stability of a-ZTO as the amorphous channel material of TOS TFTs. This would improve the device uniformity and long-term reliability of the TFTs over the very large panel area of modern flat panel displays.

This work was partly supported by the IT R&D program of MOTIE/KEIT (10035320, Development of novel 3D stacked devices and core materials for the next generation flash memory), the Converging Research Center Program through the Ministry of Science, ICT & Future Planning (2013K000159), and the KIST Institutional Program (2E24001 and 2E24070). The authors would also like to acknowledge the support from the KISTI supercomputing center through the strategic support program for supercomputing application research (KSC-2012-C2-13).

[1]P. Görrn, M. Sander, J. Meyer, M. Kröger, E. Becker, H.-H. Johannes, W. Kowalsky, and T. Riedl, Adv. Mater. **18**, 738 (2006).
[2]H. Q. Chiang, J. F. Wager, R. L. Hoffman, J. Jeong, and D. A. Keszler, Appl. Phys. Lett. **86**, 013503 (2005).
[3]B. S. Yang, S. Park, S. Oh, Y. J. Kim, J. K. Jeong, C. S. Hwang, and H. J. Kim, J. Mater. Chem. **22**, 10994 (2012).
[4]S. H. Rha, J. Jung, Y. S. Jung, Y. J. Chung, U. K. Kim, E. S. Hwang, B. K. Park, T. J. Park, J.-H. Choi, and C. S. Hwang, Appl. Phys. Lett. **100**, 203510 (2012).
[5]J. Lee, D.-Y. Cho, J. Jung, U. K. Kim, S. H. Rha, S.-C. Lee, C. S. Hwang, and J.-H. Choi, Appl. Phys. Lett. **102**, 242111 (2013).

[6]J. Heo, S. B. Kim, and R. G. Gordon, Appl. Phys. Lett. **101**, 113507 (2012).
[7]Y. Hayashi, K. Kondo, K. Murai, T. Moriga, I. Nakabayashi, H. Fukumoto, and K. Tominaga, Vacuum **74**, 607 (2004).
[8]D. L. Young, H. Moutinho, Y. Yan, and T. J. Coutts, J. Appl. Phys. **92**, 310 (2002).
[9]T. Kamiya, K. Nomura, and H. Hosono, J. Disp. Technol. **5**, 273 (2009).
[10]A. Walsh, J. L. F. Da Silva, and S.-H. Wei, Chem. Mater. **21**, 5119 (2009).
[11]T. Kamiya, K. Nomura, and H. Hosono, Phys. Status Solidi A **207**, 1698 (2010).
[12]H.-K. Noh, K. J. Chang, B. Ryu, and W.-J. Lee, Phys. Rev. B **84**, 115205 (2011).
[13]H.-H. Nahm, Y.-S. Kim, and D. H. Kim, Phys. Status Solidi B **249**, 1277 (2012).
[14]G. Kresse and J. Furthmüller, Phys. Rev. B **54**, 11169 (1996).
[15]G. Kresse and J. Furthmüller, Comput. Mater. Sci. **6**, 15 (1996).
[16]P. E. Blöchl, Phys. Rev. B **50**, 17953 (1994).
[17]J. P. Perdew, K. Burke, and M. Ernzerhof, Phys. Rev. Lett. **77**, 3865 (1996).
[18]J. Im, E. Cho, D. Kim, H. Horii, J. Ihm, and S. Han, Phys. Rev. B **81**, 245211 (2010).
[19]Y. Ding, P. X. Gao, and Z. L. Wang, J. Am. Chem. Soc. **126**, 2066 (2004).
[20]S. H. Sun, G. W. Meng, M. G. Zhang, X. H. An, G. S. Wu, and L. D. Zhang, J. Phys. D: Appl. Phys. **37**, 409 (2004).
[21]V. I. Anisimov, J. Zaanen, and O. K. Andersen, Phys. Rev. B **44**, 943 (1991).
[22]S. L. Dudarev, G. A. Botton, S. Y. Savrasov, C. J. Humphreys, and A. P. Sutton, Phys. Rev. B **57**, 1505 (1998).
[23]F. Oba, M. Choi, A. Togo, A. Seko, and I. Tanaka, J. Phys.: Condens. Matter **22**, 384211 (2010).
[24]A. K. Singh, A. Janotti, M. Scheffler, and C. G. Van de walle, Phys. Rev. Lett. **101**, 055502 (2008).
[25]A. Seko, F. Oba, and I. Tanaka, Phys. Rev. B **81**, 054114 (2010).
[26]J. Lee, S.-C. Lee, C. S. Hwang, and J.-H. Choi, J. Mater. Chem. C **1**, 6364 (2013).
[27]D.-Y. Cho, J. Song, K. D. Na, C. S. Hwang, J. H. Jeong, J. K. Jeong, and Y.-G. Mo, Appl. Phys. Lett. **94**, 112112 (2009).
[28]Y. Kang, Y. Cho, and S. Han, Appl. Phys. Lett. **102**, 152104 (2013).
[29]N. Baguer, V. Georgieva, L. Calderin, I. T. Todorov, S. V. Gils, and A. Bogaerts, J. Cryst. Growth **311**, 4034 (2009).
[30]R. M. Van Ginhoven, H. Jónsson, and L. R. Corrales, Phys. Rev. B **71**, 024208 (2005).
[31]K. Momma and F. Izumi, J. Appl. Crystallogr. **44**, 1272 (2011).
[32]C. W. Ow-Yang, D. Spinner, Y. Shigesato, and D. C. Paine, J. Appl. Phys. **83**, 145 (1998).
[33]C. A. Hoel, T. O. Mason, J.-F. Gaillard, and K. R. Poeppelmeier, Chem. Mater. **22**, 3569 (2010).
[34]N. Ito, Y. Sato, P. K. Song, A. Kaijio, K. Inoue, and Y. Shigesato, Thin Solid Films **496**, 99 (2006).
[35]C. A. Hoel, S. Xie, C. Benmore, C. D. Malliakas, J.-F. Gaillard, and K. R. Poeppelmeier, Z. Anorg. Allg. Chem. **637**, 885 (2011).